

# Role of Al<sup>3+</sup> in Enhancing the Physical Properties of Sodium Para-Nitrophenolate Dihydrate Crystals for Optoelectronic and Nonlinear Optical Applications

S. Shek Dhavud<sup>a</sup>, J. Thomas Joseph Prakash<sup>\*,b</sup>

<sup>a</sup>PG and Research, Department of Physics, Jamal Mohamed College (Autonomous), Affiliated to Bharathidasan University, Trichy, Tamilnadu, India

<sup>b</sup>PG and Research Department of Physics, Government Arts College, Affiliated to Bharathidasan University, Trichy, Tamilnadu, India

## ABSTRACT

The semiorganic nonlinear optical single crystals of undoped and Al<sup>3+</sup> doped sodium para-nitrophenolate dihydrate (SPNPD) were effectively grown by a conventional slow evaporation solution growth technique at room temperature. FT-IR spectrum shows various functional groups that are due to fundamental overtones of Al<sup>3+</sup> and SPNPD entities. The crystallinity of the materials is affirmed by powder XRD investigation. Single crystal XRD demonstrates that undoped and doped crystals have orthorhombic crystal system with space group *Ima2*. The optical absorption analyses showed that the absorption edge shifted towards lower wavelengths with the incorporation of Al<sup>3+</sup> content. The color centered emissions in the grown crystals have been tested by the photoluminescence study. Surface morphological changes because of doping are observed by SEM analysis and incorporation of dopant into the crystalline matrix of SPNPD even at the low concentrations was well affirmed by energy dispersive X-ray spectroscopy (EDAX). TG/DTA investigations were performed to study the thermal behaviour of the samples. The notable enhancement in mechanical strength was remarked due to doping. The SHG measurements also carried out on undoped and doped samples, which reveal the relative SHG efficiency has been enhanced due to doping.

**Keywords:** Nonlinear optics, Semiorganic, Photoluminescence, EDAX.

## I. INTRODUCTION

In ultra-modern years, semiorganic complexes have influenced the scientist owing to their applications in second and higher harmonic generation, optical bistability, laser remote sensing, optical disc data storage, laser-driven fusion, medical and spectroscopic image processing, color display and optical communication [1,2]. Owing to absence of prolonged p-electron delocalization and consequently moderate optical nonlinearity, low laser damage threshold, low optical transparency, lack of quality and bulk size are the main limitations in organic nonlinear optical crystals. Consequently, the research scientist that specializes in new kind of crystals named the semiorganic crystal. In semiorganic crystal, the stoichiometric bond is amongst inorganic and organic molecules provides the benefit of

combined properties such as high optical nonlinearity, prolonged transparency region-down to ultraviolet, promising crystal growth characteristics, chemical inertness and good mechanical hardness [3]. To improve the strong mechanical and high thermal stabilities in semiorganic, the cation of hydrogen-bonded nonlinear organic molecules is connected to the anion of inorganic molecules as an acid-base interaction [4]. Highly delocalized  $\pi$ -electrons yields molecular charge transfer in semiorganic that achieve  $\pi$ -electrons simply move between the electron donor and electron acceptor groups on opposite sides of the molecule [5,6].

Para-nitrophenol (C<sub>6</sub>H<sub>5</sub>NO<sub>3</sub>) could be a phenolic compound which has a nitro group at the opposite position of the hydroxyl group on the benzene ring and it is organic material whose derivatives with alkali metal hydroxides are remarkable candidates as they are a typical one-dimensional donor-acceptor  $\pi$  system. The

presence of phenolic OH supports the establishment of salts with several organic and inorganic bases [7,8] and its electron donor substituents –OH, electron acceptor substituents –NO<sub>2</sub> and phenyl group make a conjugated molecular configuration [9,10]. In this association, a semiorganic nonlinear material: Sodium p-nitrophenolate dihydrate [Na(C<sub>6</sub>H<sub>4</sub>NO<sub>3</sub>)]<sub>2</sub>.2H<sub>2</sub>O has the  $\pi$ -electron cloud changing from donor to acceptor leads to intermolecular charge transfer interaction and hence makes it non-centrosymmetric. Crystals which have non-centrosymmetric structure that exhibit both SHG and piezoelectric effects [11]. Sodium p-nitrophenolate dihydrate (SPNPD) has been described realistically in terms of crystal growth and its NLO properties [12-15]. Doping could be a very much acknowledged method for desired properties in host material for technological applications and the method have been extensively employed for enhancing the properties like electrical conductivity, growth, optical, mechanical, structural properties. It has also been recognized that specifically the metal ion dopants are the most versatile in modifying the properties of a compound [16,17]. In the series of metal ion dopants such as monovalent, divalent and trivalent, the trivalent metal ion dopant (Fe<sup>3+</sup>) in the SPNPD crystal is reported to bring on noteworthy modifications in optical, dielectric, ferroelectric, piezoelectric and nonlinear optical properties [18]. To best of our knowledge, the trivalent metal dopant (Fe<sup>3+</sup>) is the only one reported work on doped SPNPD crystals. Impact of trivalent metal ion impurities has a potential to enhance the properties of crystals as there is reported on the enhancement of various physical properties of crystals [19]. In view of the importance of trivalent ion metal dopants, Al<sup>3+</sup> ion was chosen as a dopant in the present study and we attempt to grow undoped and Al<sup>3+</sup> doped SPNPD crystals with low concentration by low-cost slow evaporation solution growth technique. In this manuscript, we have examined the effect of Al<sup>3+</sup> doping on the growth, structural, spectral, optical, Photoluminescence spectral, microstructural morphology, thermal, mechanical and SHG properties of the SPNPD crystals. All the results demonstrate that Al<sup>3+</sup> doped SPNPD crystal is promising candidate in optoelectronic and NLO applications.

## II. EXPERIMENTAL DETAILS

### 2.1. Synthesis and crystal growth

Commercially available the salts of p-nitrophenol and sodium hydroxide were employed in the present examination to synthesis Sodium p-nitrophenolate dihydrate in the molar ratio of 1:1 by dissolving it in Merck Millipore 18 M $\Omega$  cm<sup>-1</sup> resistance, deionized water, and the constant stirring was done at 50°C for 6 hours to ensure a homogeneous and saturated solution. After preparing the saturated solution, it was filtered through a Whatman filter paper and kept in a constant temperature bath at 40°C with an accuracy of 0.01°C for evaporation. After 23 days, the undoped crystal of SPNPD obtained from the bottom of the beaker it is again dissolved in deionized water, and then crystallized by controlled evaporation. Well-defined yellow colored transparent crystal was formed within 31 days. In the case of PEG additive in SPNPD crystal, the saturated solution of undoped SPNPD prepared from the good quality crystal obtained from the recrystallization process, and in this solution 0.5 mol% of Aluminium sulfate, Al<sub>2</sub>(SO<sub>4</sub>)<sub>3</sub> is added and stirred well for 6 hours for homogenization and it is filtered by Whatman filter paper and it was kept for evaporation in a dust and vibration free zone. After 22 days, the crystal with yellow colored and good transparency was harvested. The photographs of the grown crystals of undoped and 0.5 mol% of Al<sup>3+</sup> doped SPNPD crystals are presented in Fig. 1 (a) and (b).

### 2.2. Characterization techniques

The single crystal XRD investigation of undoped and doped SPNPD crystals was recorded on ENRAF NONIUS CAD 4 diffractometer with MoK $\alpha$  radiation ( $\lambda=0.71073$  Å) to recognize the unit cell parameters. Powder XRD analysis of undoped and doped SPNPD was noted on X'pert PRO powder X-ray diffraction (40 kV) by Cu-K $\alpha$  radiation of wavelength  $\lambda = 1.5406$  Å. The presence of functional groups, absorption peaks and nature of the bonds present in the undoped and Al<sup>3+</sup> doped SPNPD crystals were checked by FT-IR spectral analysis using PERKIN ELMER RXI FTIR spectrophotometer. To assess its suitability for NLO applications, undoped and doped SPNPD single crystals with a thickness of about 2 mm was subjected to UV-Vis-NIR analysis at room temperature in the wavelength range from 190 to 1100 nm using a PERKIN ELMER LAMBDA 35 UV-Visible spectrophotometer. Photoluminescence emission spectra of undoped and doped SPNPD were recorded using a Perkin Elmer LS-55 spectrometer. The scanning

electron microscope (VEGA3 TESCAN) equipped with energy dispersive analytical X-ray unit (EDAX) was employed to analysis the surface morphology and the presence of the dopant in the grown crystals respectively. In the present work, the simultaneous TG/DTA of undoped and Al<sup>3+</sup> doped SPNPD crystals were observed using a Perkin-Elmer thermal analyzer STA 409 PC in the nitrogen atmosphere under 1000 °C at a heating rate 20K/min. Vicker's microhardness measurements have checked by the utilization of Leitz Weitzler hardness tester fitted with a diamond indenter. In order to confirm the impact of doping on the NLO properties, undoped and Al<sup>3+</sup> doped SPNPD crystals have been subjected to a Q-switched Nd:YAG laser beam of wavelength 1064 nm was hired within an input beam energy of 3.2 mJ/pulse and pulse width of 8 ns, the repetition rate being 10 Hz and KDP was taken as the reference material.

### III. RESULTS AND DISCUSSION

#### 3.1. Functional group analysis

FT-IR spectroscopic analysis could be a novel instrument to check the existence of vibrational modes in inorganic, organic, as well as semiorganic compounds and it is additionally a remarkable technique to identify the impact of dopants on the vibrational modes of any material. The recorded FT-IR spectra of undoped and Al<sup>3+</sup> doped SPNPD crystals have been presented in Fig. 2, it is clear from the figure that there is a broad envelope conveying peaks owing to H-O-H stretch at 3420 and 3430 cm<sup>-1</sup> owing to hydrogen-bonded lattice water for undoped and doped SPNPD crystals respectively. Also, the vibration mode observed at 1572 and 1577 cm<sup>-1</sup> for undoped and doped SPNPD crystals was assigned to the bending mode of H-O-H. The wavenumbers such as 1462, 1308, 1115 cm<sup>-1</sup> for undoped and 1467, 1312, 1120 cm<sup>-1</sup> for doped were found owing to the presence of in-plane OH deformation. Torsion vibrations of the ring arise at 702 and 705 cm<sup>-1</sup> for undoped and doped SPNPD crystals respectively. The wavenumbers were noted at 462 cm<sup>-1</sup> for undoped and 470 cm<sup>-1</sup> for doped owing to wagging vibration of Na-OH<sub>2</sub>. These vibrational bands affirm the existence of sodium atom which was coordinated with the water molecule [20, 21]. Usually, the coordination of a metal ion with an aromatic NO<sub>2</sub> group can arise in two modes. The first one contains the metal coordination with the nitrogen atom which is often

named as nitro complex and next one contains the coordination with oxygen atom which is often called as nitrito complex. The NO<sub>2</sub> symmetric stretching vibrations are noted at 1343 and 1349 cm<sup>-1</sup> and asymmetric stretching vibrations arise at 1488 and 1495 cm<sup>-1</sup> respectively. Out-of-plane symmetric deformation of C-H bond arises at 758 and 762 cm<sup>-1</sup> for the title materials. The vibration mode found at 1172 and 1176 cm<sup>-1</sup> was assigned to in-plane bending vibrations of C-H bond for the grown crystals while out-of-plane bending vibration of C-H bond observed at 825 and 854 cm<sup>-1</sup> for undoped and for doped crystals observed at 832 and 858 cm<sup>-1</sup>. The vibration assignments of undoped and doped crystals are presented in Table 1. All the vibrational modes found in FT-IR spectra are observed to be in good agreement with the values given in the literature [22]. The slight shift in the peak positions in the vibration and stretching modes offers the experimental evidence of the incorporation of doping in SPNPD crystal lattice.

#### 3.2. X-ray diffraction analysis

The recorded powder XRD patterns of undoped and Al<sup>3+</sup> doped SPNPD crystals are exhibited in Fig. 3(a). From Fig. 3(a), it seems that there is no modification in the basic structure of the grown crystals of powder XRD patterns. No new peaks or phases were observed by doping with Al<sup>3+</sup> but variations in intensities are observed. To examine the impact of Al<sup>3+</sup> doping on peak position, we have intense on main peak (011) as indicated in Fig. 3 (b) which evidently depicts that the there is a considerable change in peak position and also the intensity of the main peaks has been increased. The well-defined Bragg's peaks at specific 2θ angles exhibit a high crystallinity of samples. The ionic radius of the dopant Al<sup>3+</sup> (53 pm) is very small compared with that of Na<sup>+</sup> (102 pm) [23]. Therefore, it is reasonable to conceive that the dopant may enter into the SPNPD crystalline matrix without producing much distortion. The slight modifications in the lattice parameters exhibit the lattice strain due to the doping.

#### Determination of crystallite size by Scherrer analysis

The crystallite size of undoped and doped SPNPD crystals was estimated from the Scherrer equation

$$D = \frac{k\lambda}{\beta_D \cos \theta} \text{----- (1)}$$

Where  $D$  is the volume weighted crystallite size (nm),  $k$  is the shape factor ( $k = 0.9$ ),  $\lambda$  is the wavelength of the X-rays ( $k = 1.54056 \text{ \AA}$  for Cu  $K\alpha$ ),  $\theta$  is Bragg diffraction angle and  $\beta_D$  is the Full width at half-maximum intensity (FWHM) in radians. The crystallite size of crystalline domains which diffract coherently is decreased from 51 nm (for undoped SPNPD) to 23 nm (for  $\text{Al}^{3+}$  doped SPNPD crystals).

From the single crystal XRD analysis, it was noted that undoped and doped SPNPD crystals belong to an orthorhombic crystallographic system with space group  $\text{Ima}2$  and the unit cell parameters of the doped sample exhibit slight variations shown in Table 2. From Table 2, it is clear that the unit cell volume is found to be increased compared to undoped SPNPD which is also a strong indication of  $\text{Al}^{3+}$  doping into the crystalline matrix of SPNPD crystals. The single XRD data is in good agreement with the values given in the literature [12].

### 3.3. UV–Vis–NIR absorption studies

The absorption spectrum is extremely vital for any NLO material because a nonlinear optical material may be of practical utilizes just in the event that it has wide transparency window. The absorption spectra of undoped and doped SPNPD crystal are shown in Fig. 4 (a) and (b). As shown in Fig. 4 (b),  $\text{Al}^{3+}$  doped SPNPD crystal is seen to have low absorption between the wavelength 470 and 1100 nm compared to undoped SPNPD crystal and better transparency in the entire visible region which has good agreement with the literature [24]. The low absorption in the entire region from 470 nm to 1100 nm empowers it to be a good candidate for electro-optic and NLO applications. In the doped crystal, there was a sudden increment in absorption at the wavelength just below 470 nm owing to the electronic transitions in the aromatic ring of the title material and also due to the colour of the crystal.

### 3.4. Photoluminescence analysis

Photoluminescence spectra of undoped and doped SPNPD crystals were noted at room temperature by way of exciting it at 450 nm. The PL emissions are observed for undoped and  $\text{Al}^{3+}$  doped SPNPD crystals overlaying from the very short wavelength of 400 nm to long wavelength 600 nm as shown in Fig. 5 (a) and (b). The recorded spectra fitted by means of Gaussian function

with three peaks for both undoped and doped crystals. The emission spectra of undoped and  $\text{Al}^{3+}$  doped SPNPD crystals are having three peaks at (515, 529 and 541 nm) and (518, 532 and 545 nm) respectively. These bands are just green emission for both the crystals. Further, we have noticed that emission intensity is strongly influenced by using the adding dopant. From Fig. 5 (b), the PL intensity of the doped sample is markedly higher than that of undoped SPNPD crystals.

### 3.5. Microstructural Morphology and Energy dispersive X-ray analysis

Fig. 6(a) and (b) indicates the SEM images of as grown single crystals of undoped and doped SPNPD crystals. The SEM images show that undoped and  $\text{Al}^{3+}$  doped SPNPD crystals exhibit transparent nature with smooth surfaces. More scatter centers were found in the doped sample compared to the undoped ones.  $\text{Al}^{3+}$  doped SPNPD crystal exhibits a film like morphology with the grains of a size of the order of few micrometers (20  $\mu\text{m}$ ) on the surface whereas for undoped SPNPD crystal the grains of a size of the order of micrometers (50  $\mu\text{m}$ ) on the surface. The obtained results coincide well with the powder XRD analysis (section 3.2). The percentage of  $\text{Al}^{3+}$  is clear in the EDAX spectra as shown in Fig. 6(c) and (d). From figures, the presence of C, O and Na intense peaks are present which indicates the formation of  $\text{Al}^{3+}$  doped SPNPD single crystal. In comparison with undoped SPNPD crystal, it is observed that the EDAX which identifies the incorporation of  $\text{Al}^{3+}$  in the crystal lattice of SPNPD shown in Fig. 6 (c) and (d). It discloses that the accommodating capability of the host crystal is limited and only a small quantity is incorporated into the crystalline matrix.

### 3.6. Thermal stability studies

Thermal examinations have been carried out on the samples of grown crystal to investigate the thermal stability and melting point as they provide thermal stability of the materials. In the course of the device fabrication, a significant amount of heat is generated while cutting and polishing the crystals and heat will also be generated during the continuous laser exposure. Therefore, it's vital to review the thermal stability of the grown crystals. The experiment has been performed in a nitrogen atmosphere and the TG & DTA plots are as shown in Fig. 7 (a) and (b). There's a weight loss below 125  $^\circ\text{C}$  in undoped and doped grown crystals which is

assigned to loss of water in the TGA curve. A careful investigation of TG curve for samples indicates the weight loss in two stages. For the undoped crystal, it arises below 120 °C and for doped crystal, it arises below 127 °C due to the removal of strongly and weakly entrapped lattice water respectively. The sharp peak observed at 353.3 °C and 362.5 °C in Fig. 7 (a) and (b) is owing to the melting point of undoped and doped crystals respectively. Thermal stability of the doped specimen is slightly enhanced by doping with Al<sup>3+</sup> (362.5 °C) in comparison with the thermally stable temperature for undoped SPNPD (353.3 °C) and reported earlier for pure SPNPD (342 °C) [25]. No decomposition till the melting point ensures the suitability of the material for application in lasers where the crystals are required to withstand high temperatures.

### 3.7. Mechanical stability studies

The hardness parameters play a vital role once they are employed for optical device applications. Consequently, it looks to be essential to reveal mechanical properties of undoped and Al<sup>3+</sup> doped SPNPD crystals. Vickers microhardness values were calculated from the relation

$$H_V = 1.8544 P / d^2 \text{ (Kg/mm}^2\text{)} \quad \text{----- (2)}$$

Where, P – Applied load in gram and d – The average diagonal length of indentation mark in the micrometer. Fig. 8 represents the hardness values of the grown crystals as a function of load. The hardness values increased with increase in load for undoped and doped SPNPD crystals. The observed increase in hardness values with increasing load for all the examined samples are often understood based on the reverse indentation size effect (RISE). The hardness values of Al<sup>3+</sup> doped crystal have higher than that of undoped crystal. The explanation behind the higher hardness in the doped crystal could be comprehended viz., the addition of the Al<sup>3+</sup> impurity has a noticeable impact on the hardness of polymer crystals. The mechanical strength of doped SPNPD crystal might favor advantage of less breakage and crack in the course of processing the material while fabricating technological devices [26]. The increase in hardness value is owing to the work hardening of surface layers, and the RISE may be subjected to the generation of cracks around the indentation. The work hardening coefficient or Meyer's index (n) is calibrated by the least square fitting method [27] shown in Fig. 9

(a) and (b). The values of Meyer's index (n) calibrated for undoped (3.0) and Al<sup>3+</sup> doped SPNPD (4.1) crystals. Thus, the calibrated values propose that these grown crystals belong to a soft material type.

### 3.8. Second harmonic generation efficiency

In order to affirm the impact of doping on the NLO properties, the as-grown undoped and doped crystals were subjected to SHG test. The output SHG intensities of undoped and doped specimens offer the relative NLO efficiencies of the measured specimens. The doubling of frequency was affirmed by the green color of the output radiation whose characteristic wavelength is 532 nm. Green color emission specifies that the doped material exhibits second order NLO effect. The second harmonic signals of undoped and doped crystals are 36 mV and 38 mV. The relative measured NLO output of undoped and doped SPNPD crystals are 5.14 and 5.42 times with respect to KDP respectively. A slight enhancement of SHG efficiency at low doping levels of Al<sup>3+</sup> could be owing to the easy of charge transfer. The SHG efficiency measured in doped SPNPD crystal is high in comparison to reported work on pure and Fe<sup>3+</sup> doped SPNPD crystals [18]. The enhancement of SHG efficiency owing to Al<sup>3+</sup> doping makes it more suitable than undoped as well as many other materials (Fe<sup>3+</sup>) for optoelectronic device fabrication.

## IV. CONCLUSION

Undoped and Al<sup>3+</sup> doped nonlinear optical SPNPD crystals were grown by a slow evaporation solution growth technique. Single crystal XRD examination affirms that the crystals belong to orthorhombic crystal structure with Ima2 space group which remains same after the incorporation of 0.5 mol% of Al<sup>3+</sup>. Incorporation of Al<sup>3+</sup> reduces the crystal lattice owing to the presence of the interstitial spaces in the undoped crystal. From PXRD examination, the enhancement in the X-ray peaks intensity and change in peak position affirms the presence of Al<sup>3+</sup> doping in the crystalline matrix of SPNPD without a change in phase. A small variation in the FT-IR vibrational frequencies because of Al<sup>3+</sup> doping was observed. The low absorbance observed in the doped SPNPD affirms that the quality of SPNPD crystals has been remarkably enhanced owing to Al<sup>3+</sup> incorporation in SPNPD. In PL spectra, the defect level emission of Al<sup>3+</sup> doped SPNPD crystal was decreased when compared with undoped SPNPD and

the optoelectronic properties predominantly depend on the decrease of defect level in material, which impacted by electron-phonon coupling interaction and the results provide strong support for the further development of extensive optical device application. SEM micrographs reveal that the surface morphology modifications in the doped specimen. Incorporation of  $\text{Al}^{3+}$  in the crystalline matrix of SPNPD is well established by EDAX analysis. Thermal studies indicate that the thermal stability of  $\text{Al}^{3+}$  doped crystal is better than undoped ones. In the microhardness analysis, Vicker's hardness ( $H_v$ ) parameter was found to increase because of  $\text{Al}^{3+}$  doping in the SPNPD crystals. The Meyer's index ( $n$ ) was determined to be 3.0 for undoped SPNPD and 4.1 for  $\text{Al}^{3+}$  doped SPNPD suggesting that these crystals exhibit reverse indentation size effect (RISE) and belong to the type of soft materials. The NLO analysis affirms that the presence of dopant slightly enhances the efficiency of undoped SPNPD. The reasonably good optical, thermal properties combined with very high SHG efficiency suggests that undoped SPNPD crystals with  $\text{Al}^{3+}$  ion substitution can be exploited for future application in optoelectronic and NLO device fabrications.

## V. REFERENCES

- [1]. Santhanu Bhattacharya, Parthasarathi Dastidar, T.N. Guru Row, Hydrogen-bond-directed self-assembly of D-(+)-dibenzoyltartaric acid and 4-aminopyridine: optical nonlinearities and stoichiometry-dependent novel structural features, *Chem. Matter.* 6 (1994) 531-537.
- [2]. Y.J. Ding, X. Mu, X. Cu, Efficient generation of coherent blue and green light based on frequency conversion in  $\text{KTiOPO}_4$  crystals,
- [3]. *J. Nonlinear Opt. Phys. Matter.* 9 (2000) 21-53.
- [4]. N. Karthick, R. Sankar, R. Jayavel, S. Pandi, Synthesis, growth and characterization of semiorganic nonlinear optical bistiourea antimony tribromide (BTAB) single crystals, *J. Cryst. Growth.* 312 (2009) 114-119.
- [5]. C.B. Aakeroy, P.B. Hitchcock, B.D. Moyle, K.R. Seddon, Organic salts of L-tartaric acid: materials for second harmonic generation with a crystal structure governed by an anionic hydrogen-bonded network, *J. Chem. Soc. Chem. Commun.* (1992) 553-555.
- [6]. Ch. Bosshard, K. Sutter, Ph. Pretre, J. Hulliger, M. Florsheimer, P. Kaatz, P.Gunter. *Organic Nonlinear Optical Materials.* Gordon and Breach, Basel, 1995.
- [7]. M.C. Etter, Hydrogen bonds as design elements in organic chemistry, *J. Phys. Chem.* 95 (1991) 4601-4610.
- [8]. M. Thangaraj, G.Vinitha, T.C.Sabari Girisun, P.Anandan, G.Ravi, Third order nonlinear optical properties and optical limiting behavior of alkali metal complexes of p-nitrophenol, *Opt Laser Technol.* 73 (2015) 130-134.
- [9]. J. M. Harrowfield, B. W. Skelton, A. H. White, Structural studies of alkaline earth metal picrates, *Aust. J. Chem.* 48 (1995) 1333-1347.
- [10]. S. Boomadevi, R. Dhanasekaran, P. Ramasamy, Investigations on nucleation and growth kinetics of urea crystals from methanol, *Cryst. Res.Technol.* 37 (2002) 159-168.
- [11]. K. Sangwal, E. Mielniczek-Brzo'ska, Effect of impurities on metastable zone width for the growth of ammonium oxalate monohydrate crystals from aqueous solutions, *J. Cryst. Growth.* 267 (2004) 662-675.
- [12]. J. Dalal, N. Sinha, B. Kumar, Structural, optical and dielectric studies of novel nonlinear Bisglycine Lithium Nitrate piezoelectric single crystal, *Opt. Mater.* 37 (2014) 457-463.
- [13]. H. Minemoto, N. Sonoda, K. Miki, Structure of sodium p-nitrophenolate dihydrate, *Acta Cryst. C.* 48 (1992) 737-738.
- [14]. H. Minemoto, Y. Ozaki, N. Sonoda, T. Sasaki, Intracavity second-harmonic generation using a deuterated organic ionic crystal, *Appl. Phys. Lett.* 63 (1993) 3565-3567.
- [15]. H. Minemoto, Y. Ozaki, N. Sonoda, T. Sasaki, Crystal growth and the nonlinear optical properties of 4-nitrophenol sodium salt dihydrate and its deuterated material, *J. Appl.Phys.* 76 (1994) 3975-3980.
- [16]. S. Brahadeeswaran, V. Venkataramanan, J.N. Sherwood, H.L. Bhat, Crystal growth and characterization of semiorganic nonlinear optical material: sodium p-nitrophenolate dihydrate, *J. Mater. Chem.* 8 (1998) 613-618.
- [17]. V. Praveen, N. Vijayan, C. Mahadevan, G. Bhagavannarayana, Effect of impurities on the crystalline perfection of ZTS, *Mater. Manuf. Processes.* 23 (2008) 816-822.
- [18]. N. Kejalakshmy, K. Srinivasan, Growth, optical and electro-optical characterisations of potassium

- hydrogen phthalate crystals doped with Fe<sup>3+</sup> and Cr<sup>3+</sup> ions, *Opt. Mater.* 27 (2004) 389-394.
- [21]. Jyoti Dalal, Binay Kumar, Remarkable Enhancement in dielectric, piezoelectric, ferroelectric and SHG Properties by iron doping in sodium para-nitrophenolate dihydrate single crystals, *Mater. Lett.* 165 (2016) 99-102.
- [22]. P. Kanchana, A. Elakkina Kumaran, C. Sekar, Effect of trivalent metal ion impurities (Al<sup>3+</sup>, Cr<sup>3+</sup> and Fe<sup>3+</sup>) on the growth, structural and physical properties of potassium acid phthalate (KAP) crystals, *Spectrochim. Acta, Part A.* 112 (2013) 21-26.
- [23]. D. Lin-Vien, N.B. Colthup, W.G. Fatley, J.G. Grasselli, *The Handbook of Infrared and Raman Characteristic Frequencies of Organic Molecules.* Academic Press, New York, 1991.
- [24]. R.A. Nyquist, R.O. Kagel, *The Handbook of Infrared and Raman Spectra of Inorganic Compounds,* Chemical physics research laboratory. New York, 1971.
- [25]. M. Ben Salah, P. Becker, C. Carabatos-Nedelec, Raman and infrared spectra of sodium p-nitrophenolate dihydrate (NPNa), [Na(C<sub>6</sub>H<sub>4</sub>NO<sub>3</sub>)]<sub>2</sub>.2H<sub>2</sub>O, *Vib. Spectrosc.* 26 (2001) 23-32.
- [26]. R. D. Shannon, Revised Effective Ionic Radii and Systematic Studies of Interatomic Distances in Halides and Chalcogenides, *Acta Crystallogr. Sect. A.* 32 (1976) 751-757.
- [27]. B. Milton Boaz, A. Leyo Rajesh, S. Xavier Jesu Raja, S. Jerome Das, Growth and characterization of a new nonlinear optical semiorganic lithium para-nitrophenolate trihydrate (NO<sub>2</sub>-C<sub>6</sub>H<sub>4</sub>-OLi•3H<sub>2</sub>O), *J. Cryst. Growth.* 262 (2004) 531-535.
- [28]. S. Vanishri, S. Brahadeeswaran, H.L. Bhat, Crystal growth of semiorganic sodium p-nitrophenolate dihydrate from aqueous solution and their characterization, *J. Cryst. Growth.* 275 (2005) e141-e146.
- [29]. M. Anis, G.G. Muley, M.D. Shirsat, S.S. Hussaini, Single crystal growth, structural, optical, mechanical, dielectric and thermal studies of formic acid doped potassium dihydrogen phosphate crystal for NLO applications, *Cryst. Res. Technol.* 50 (2015) 372-378.
- [30]. S. Kalainathan, K. Jagannathan, Mechanical and surface analysis of stilbazolium tosylate derivative crystals, *J. Cryst. Growth.* 310 (2008) 2043-2049.

**Table 1** The vibrational modes of undoped and Al<sup>3+</sup> doped SPNPD single crystals and their tentative assignments

IR (cm <sup>-1</sup> )		Assignment
Undoped SPNPD	Al <sup>3+</sup> doped SPNPD	
3420	3430	OH stretching vibration
1462, 1308, 1115	1467, 1312, 1120	OH in-plane deformation
1343	1349	NO <sub>2</sub> symmetric stretching
1488	1495	NO <sub>2</sub> asymmetric stretching
1172	1176	C-H in-plane bending
825, 854	832, 858	C-H out-of-plane bending
758	762	C-H out-of-plane symmetric deformation (wagging)
702	705	Ring torsion
647	651	Ring bending or stretching vibration

**Table 2** Comparison of unit cell parameters of undoped and Al<sup>3+</sup> doped SPNPD single crystals

Lattice parameters	Undoped SPNPD	Al <sup>3+</sup> doped SPNPD
a (Å)	6.833	6.882
b (Å)	19.625	19.677
c (Å)	6.410	6.432
α = β = γ	90°	90°
Volume (Å) <sup>3</sup>	859.56	871

Crystal system  
Space group

orthorhombic  
Ima2

orthorhombic  
Ima2

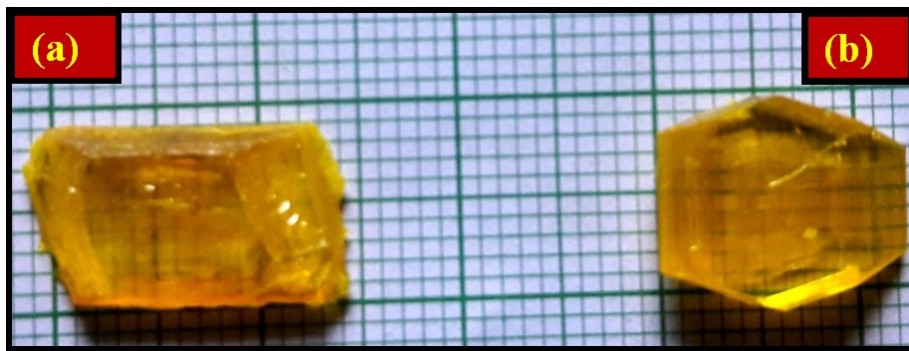


**Figure 1** As grown crystals of (a) Undoped (b)  $\text{Al}^{3+}$  doped SPNPD.

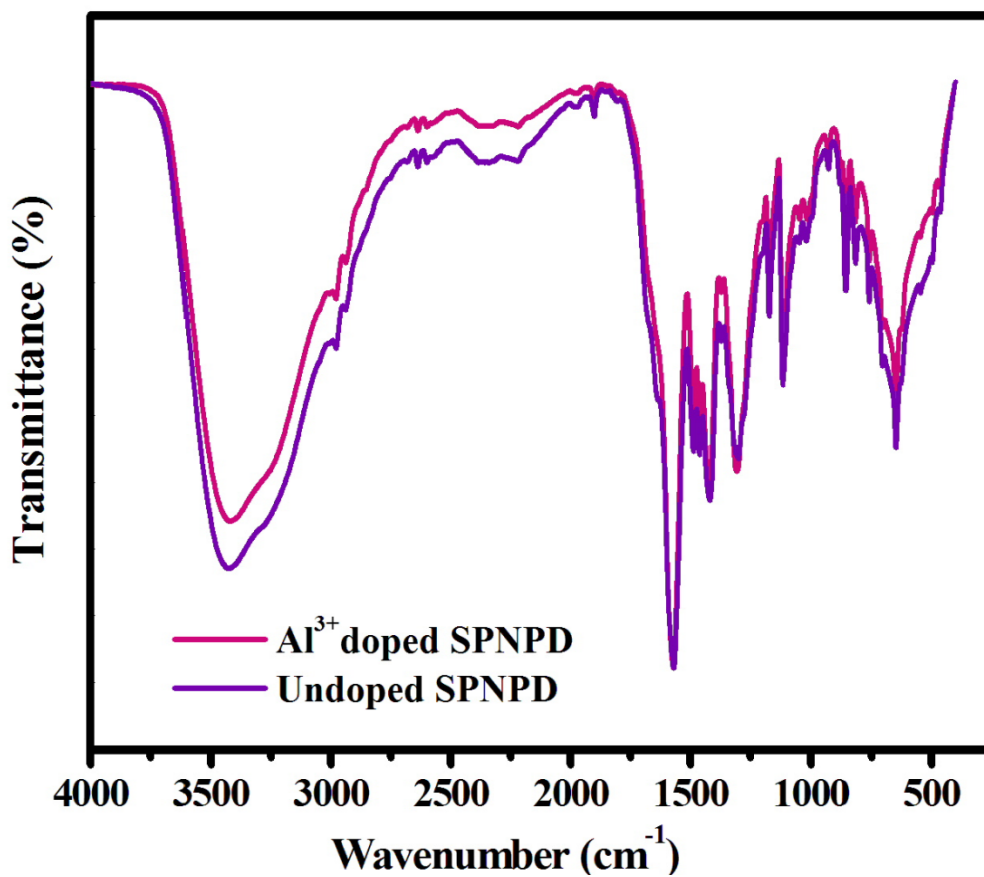


**Figure 2** FTIR spectrum of undoped and  $\text{Al}^{3+}$  doped SPNPD crystals.

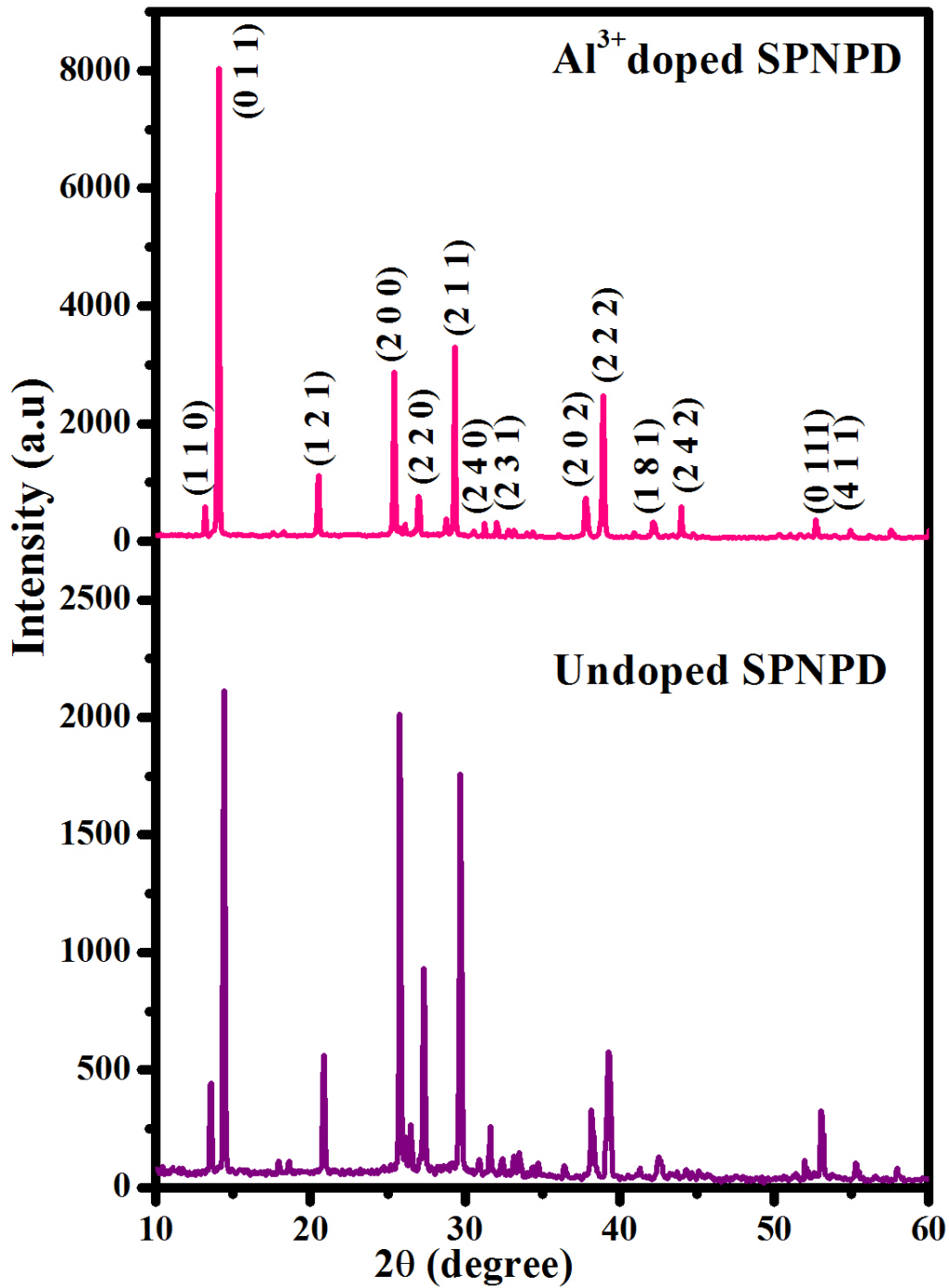


Figure 3. Powder XRD pattern of undoped and Al<sup>3+</sup> doped SPNPD crystals.

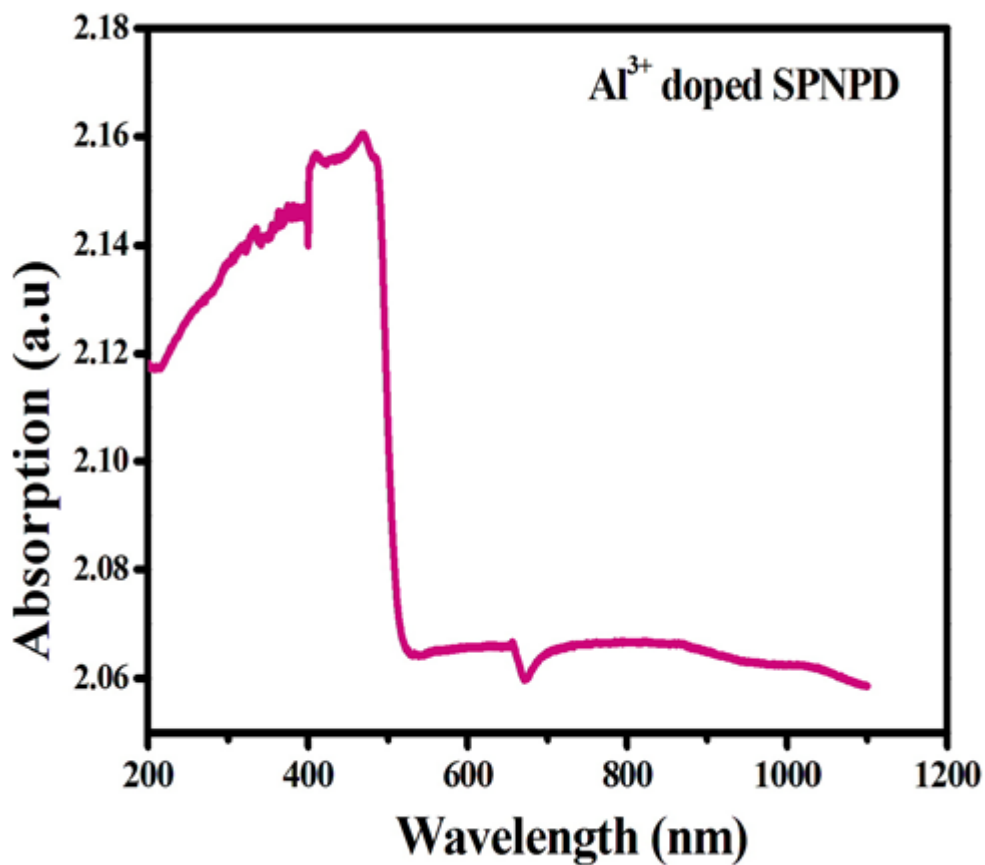
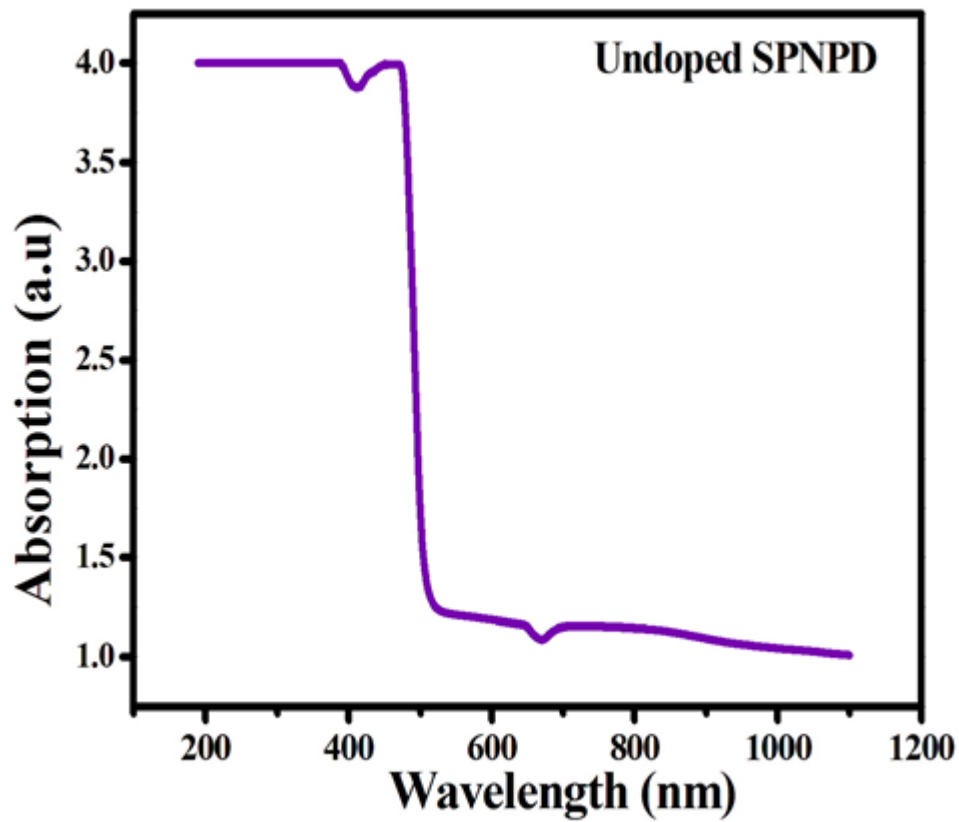
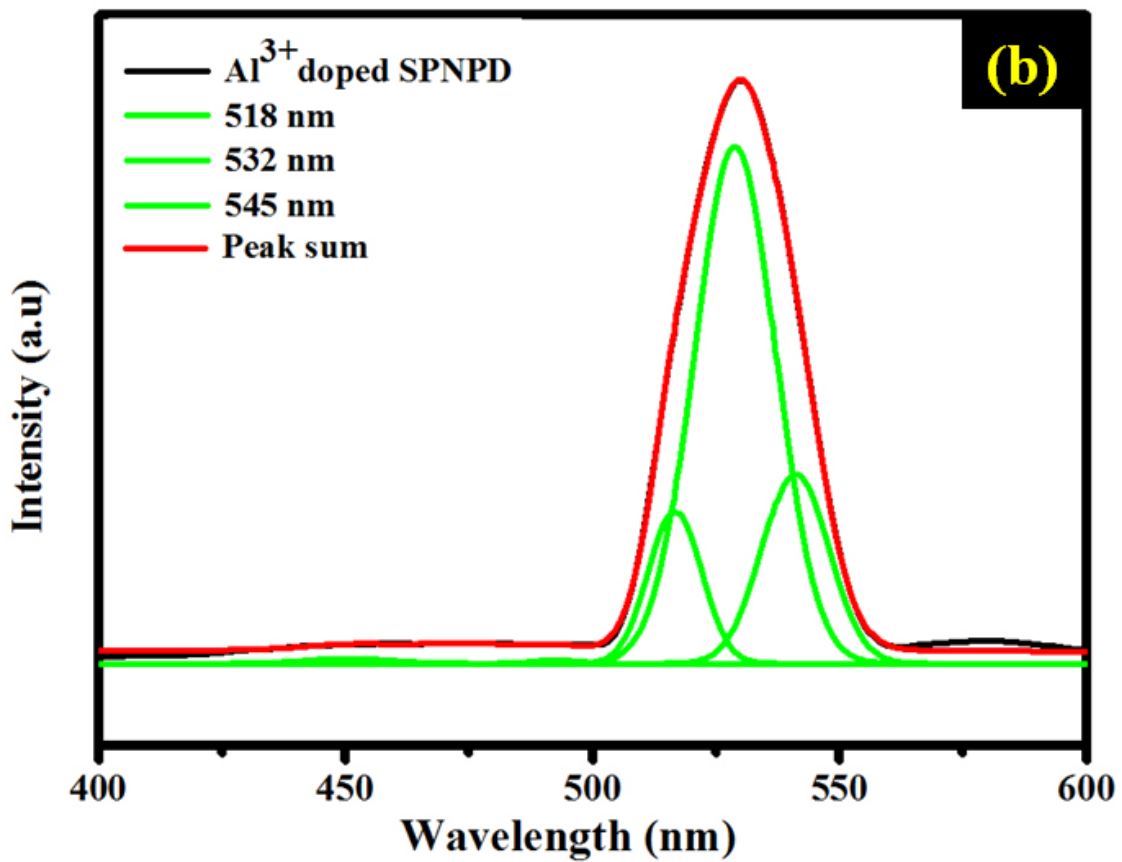
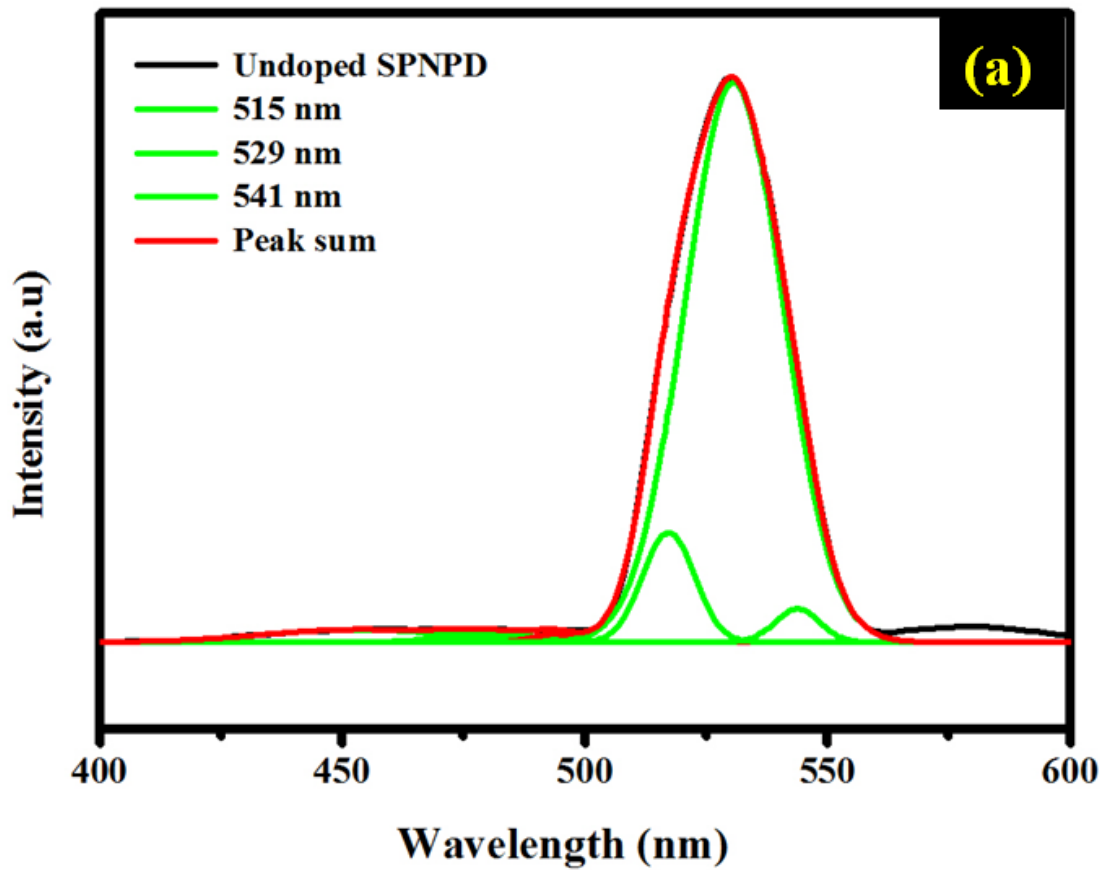
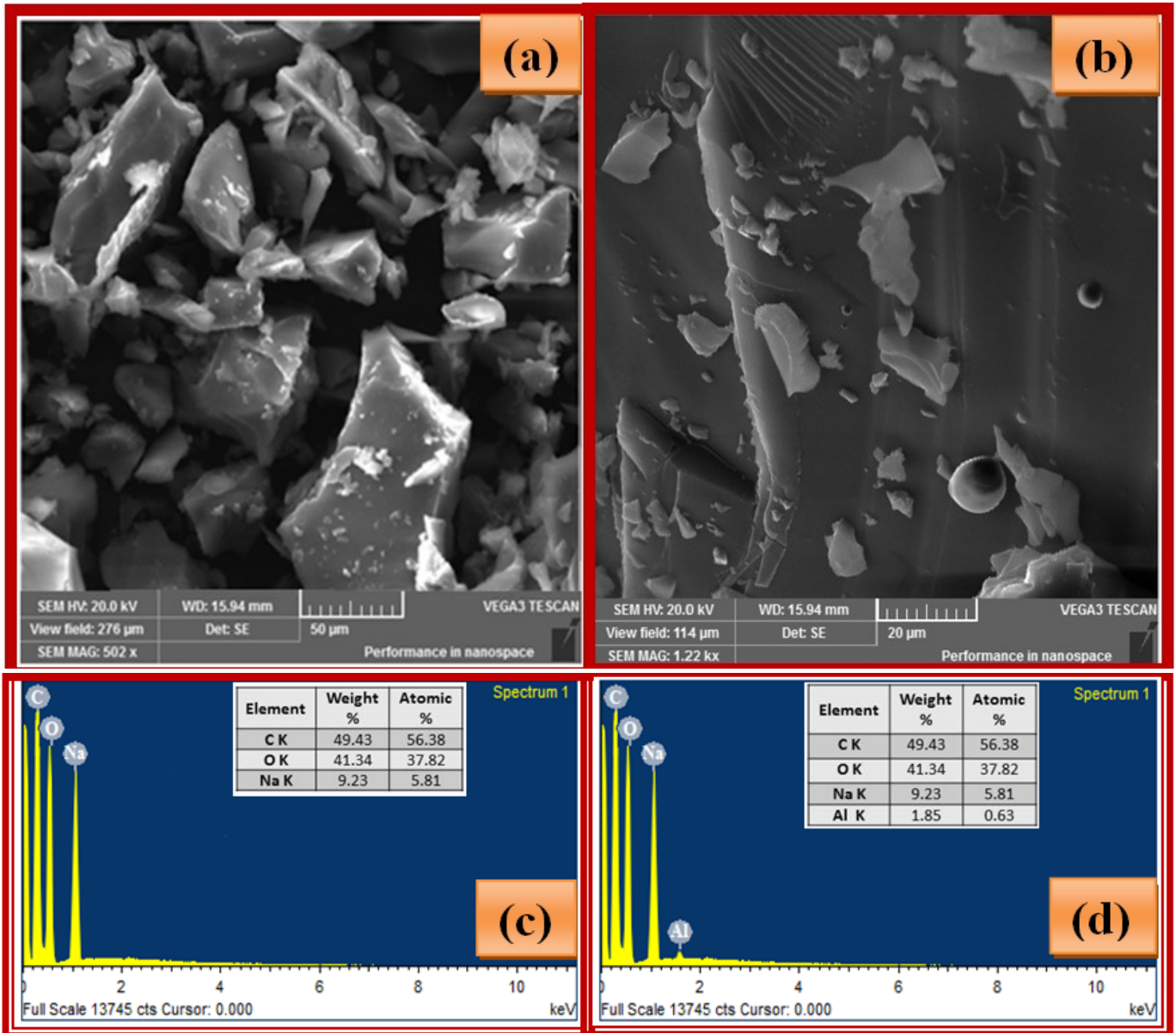


Figure 4 UV-Vis-NIR absorption spectrum of undoped and Al<sup>3+</sup> doped SPNPD crystals.



**Figure 5** Photoluminescence spectrum of (a) Undoped SPNPD crystal  
(b) Al<sup>3+</sup> doped SPNPD crystal.



**Figure 6** SEM micrographs of (a) undoped SPNPD crystal (b) Al<sup>3+</sup> doped SPNPD crystal. EDAX patterns of (c) undoped SPNPD crystal (d) Al<sup>3+</sup> doped SPNPD crystal.

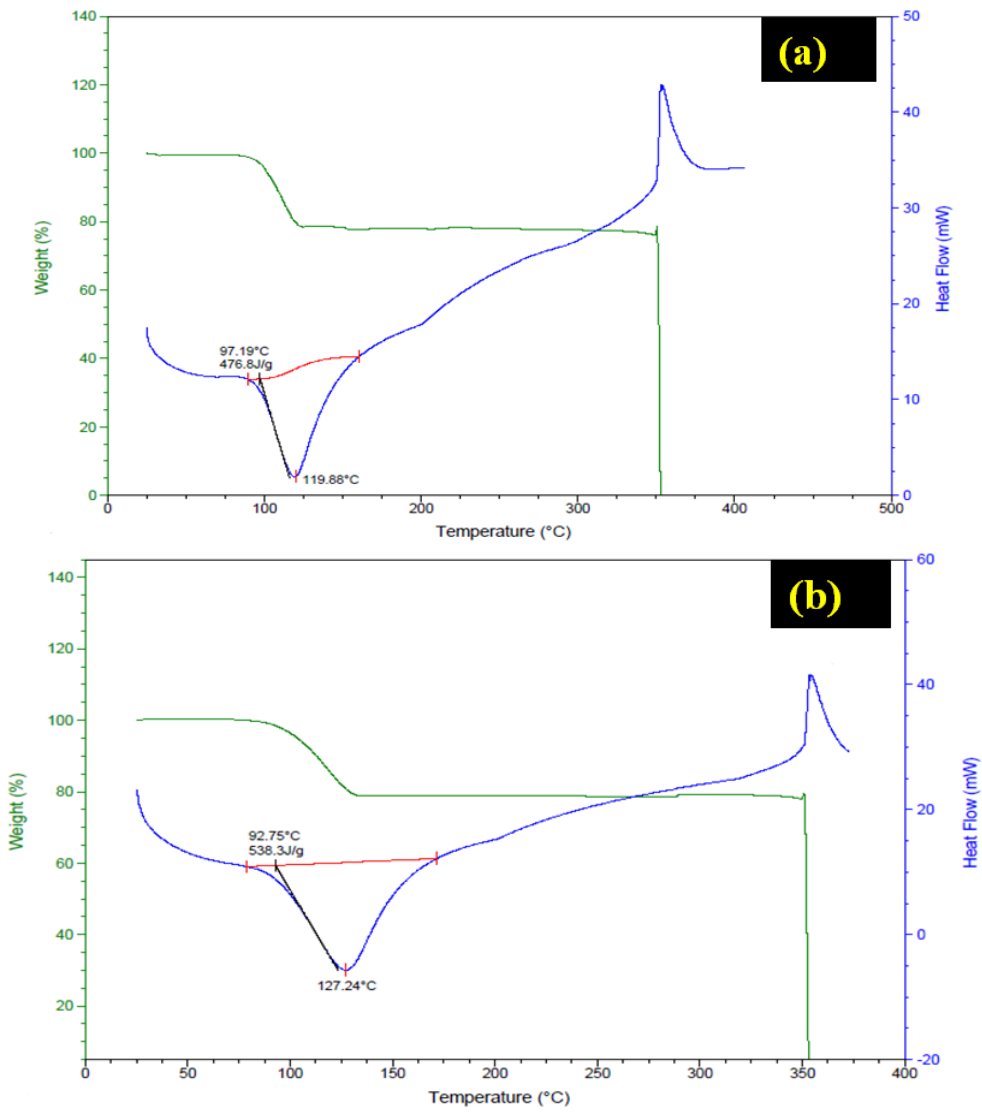


Figure 7 TG/DTA curves of (a) undoped SPNPD crystals (b) Al<sup>3+</sup> doped SPNPD crystal.

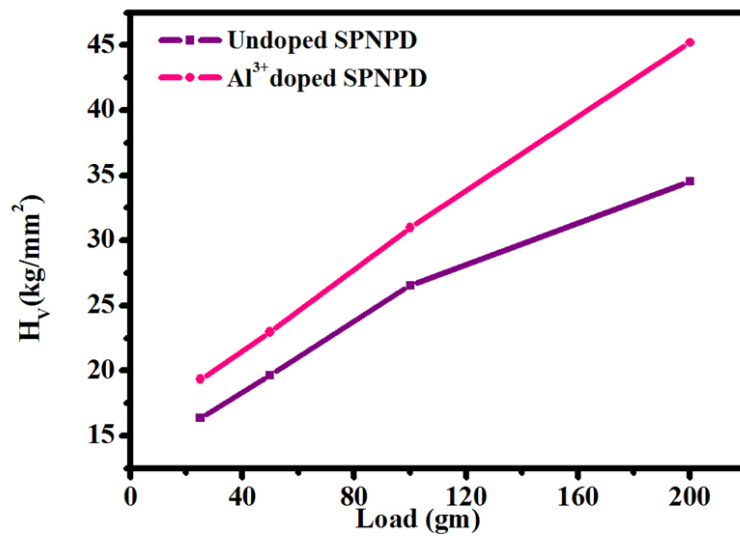
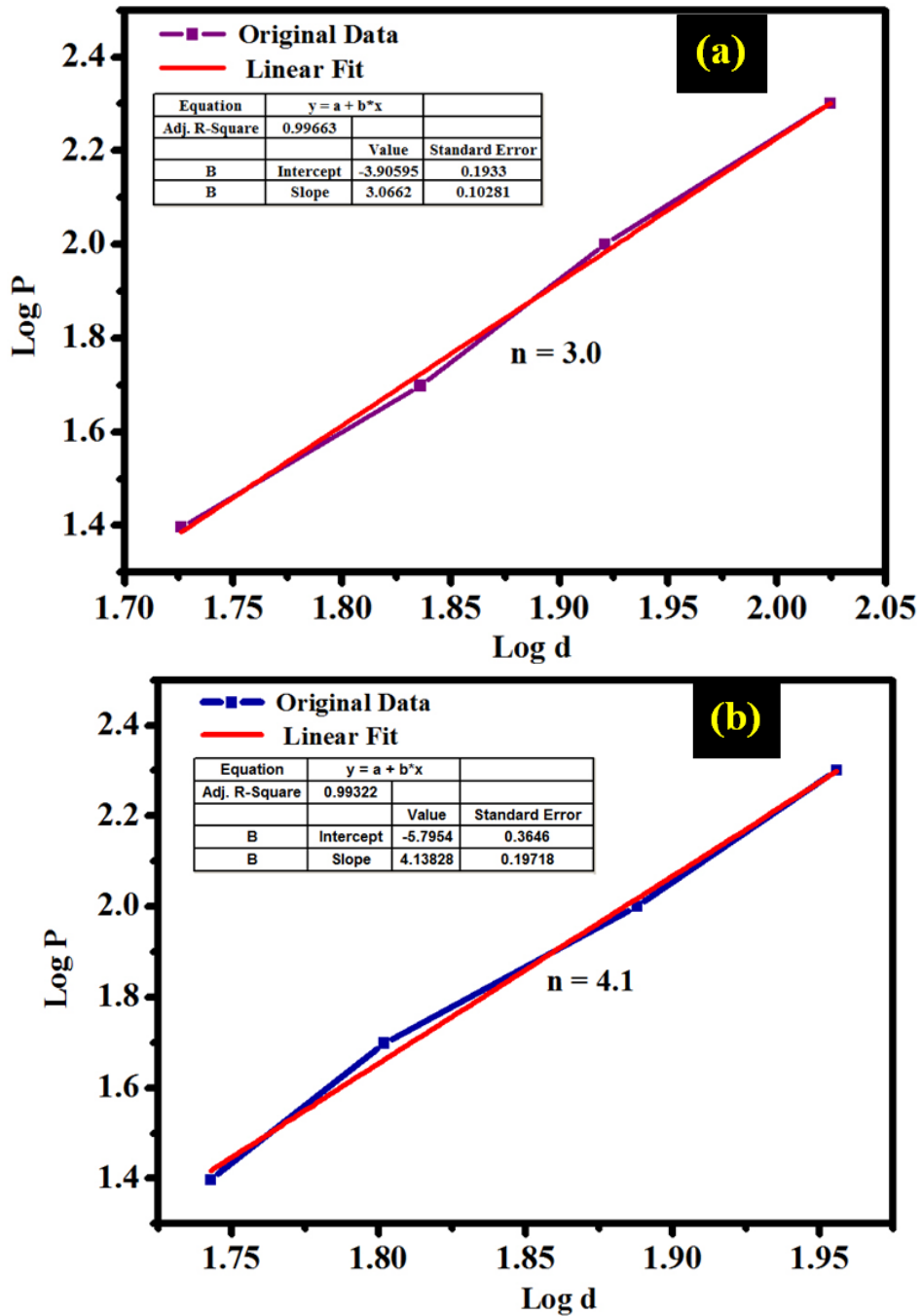


Figure 8 Load vs Hv for undoped and Al<sup>3+</sup> doped SPNPD crystals.



**Figure 9** Log P vs Log d plot of (a) undoped SPNPD crystal (b) Al<sup>3+</sup> doped SPNPD crystal.